J Mater Sci (2016) 51:7803–7813

Review

Artificial multiferroic structures based on barium-strontium titanate

Alexander A. Semenov[1], Antonina I. Dedyk[1], Andrey A. Nikitin[1], Pavel Yu. Belyavskiy[1,*], Yulia V. Pavlova[1], Ivan L. Mylnikov[1], Alexey B. Ustinov[1], Viktor V. Plotnikov[2], Andrey V. Eskov[2], Oleg V. Pakhomov[2], and Andrey A. Stashkevich[3,2]

[1] *Department of Physical Electronics and Technology, St. Petersburg Electrotechnical University, St. Petersburg, Russia 197376*
[2] *International Laboratory "MultiferrLab", ITMO University, St. Petersburg, Russia 197101*
[3] *LSPM (CNRS-UPR 3407), Université Paris 13, Sorbonne Paris Cité, 93430 Villetaneuse, France*

Received: 11 March 2016
Accepted: 20 May 2016
Published online: 31 May 2016

ABSTRACT

Artificial extrinsic and intrinsic multiferroic structures were developed in the form of yttrium-iron garnet/barium-strontium titanate bi-layers and manganese-doped barium-strontium titanate films with a relatively high doping rate in the range of 10–20 mol%. For the experimental investigations, the planar capacitors were formed on the surfaces of the structures and the capacitance–voltage characteristics were measured. Structural characterization of the samples under study was based on X-ray diffraction analysis and film–substrate interfaces were investigated by X-ray photoelectron spectroscopy. The relative dielectric permittivity, dielectric loss tangent, and electric field tunability of the samples were measured in a temperature range from 77 to 300 K. The additional 6 and 3 % tuning of the dielectric permittivity by external magnetic field of 2000 Oe was demonstrated for the extrinsic and intrinsic structures, respectively.

Introduction

Multiferroics, i.e., materials or heterostructures, that possess more than one ferroic parameter have been intensively studied during the last two decades both theoretically and experimentally. A revival of interest in them has been mainly driven by such important potential applications as data storage devices in which advantage is taken of new functionalities originating from coupling of two constituent ferroic phases [1–9]. Typically, these are ferroelectric and ferromagnetic ones and effective magnetoelectric coupling is made possible via direct or indirect interaction between them. Magnetic-based devices, the most promising candidates for data storage and information processing, though possessing numerous indubitable advantages, are characterized by significant energy dissipation in the form of heat, which has become a major impediment in the pursuit of speed and storage density for the microelectronics industry. It has turned out that the problem can be solved by switching from magnetic to electric field in the control of the magnetic element, typically used as information structure. This is where multiferroics appear

Address correspondence to E-mail: pbeliavskiy@gmail.com

DOI 10.1007/s10853-016-0090-6

to be of inestimable value. Another branch of research activity in this field is driven by important applications to the microwave devices of multiferroic materials [5–9]. The latter fall into two major categories, namely the intrinsic/natural materials and extrinsic/artificial ones. In the media belonging to the first group, such as $BiFeO_3$, both phases, the ferroelectric and ferromagnetic, coexist simultaneously in one natural material, which can be very useful. Artificial structures made of separate ferromagnetic and ferroelectric phases mixed together in different forms are referred to in the literature as extrinsic multiferroics. They have demonstrated much more pronounced magnetoelectric features, which makes them especially promising for major applications. Typically, their properties can be independently controlled by two fields of different physical nature. The magnetic control is straightforward and is implemented through the explicit dependence of the Polder tensor elements on the applied external magnetic field [10].

At the same time, there exist two completely different physical mechanisms to realize the electric control. Ferroelectrics exist either in the high-symmetry high-temperature paraelectric phase or in the low-symmetry low-temperature ferroelectric phase. In the first case, the control of the effective parameters is implemented via direct nonlinear modulation of the dielectric permittivity by an electric field. In the latter case, it is a two-step process within which advantage is taken of pronounced piezoelectricity, typical of the ferroelectric phase and equally pronounced magnetoelastic coupling typical of the ferromagnetic phase. Thus at the first stage, the control electric field induces a static stress in the piezoelectric/ferroelectric component. It is transferred to the magnetoelastic/ferromagnetic layer, in which it induces a static magnetic field via the inverse magnetostrictive effect [10]. In the case of microwave applications, typically, the ferromagnetic layer is in the saturated state, and the above-mentioned effect consists in generation of an additional anisotropic magnetic field leading to variation of the effective magnetic magnetization due to displacement of magnetic dipoles in the crystalline lattice as a result of mechanical deformation. Since the ferroelectric phase in this configuration plays the role of a piezoelectric transducer, it can be hence replaced with any material with piezoelectric properties, not necessarily ferroelectric, like quartz.

It should be noted that each "scenario" of electric control has its undeniable advantages for a specific application. For example, the paramagnetic phase, having very low, with respect to the ferromagnetic one, microwave losses is ideally suited for high-frequency signal treatment.

As mentioned previously, the artificial extrinsic multiferroics are typically characterized by much stronger (several orders of magnitude) magnetoelectric coupling than their intrinsic analogues. In this paper, we investigate multiferroic behavior of two alternative structures, both based on barium-strontium titanate solid solutions $Ba_xSr_{1-x}TiO_3$ (BSTO). Interestingly, intrinsic multiferroic materials obtained via doping with Mn, demonstrate magnetoelectric coupling practically as strong as that of a classical extrinsic BSTO/YIG bi-layer.

Samples preparation

In what concerns microwave applications, the most promising candidates for fabrication of multiferroic structures are materials with low insertion losses at microwaves. They are well known. On the ferromagnetic side, these are single-crystal yttrium-iron garnet $Y_3Fe_5O_{12}$ (YIG) films typically grown on gallium-gadolinium garnet (GGG) substrates [11], while among ferroelectrics especially attractive are thin films of perovskite-type materials and, in particular, barium-strontium titanate solid solutions BSTO [9, 12, 13]. The x parameter describing their stoichiometry can be regarded as an additional degree of freedom, making possible customizing their properties for a given application. Microwave devices require minimization of insertion losses that are defined by $\tan\delta$ and maximization of electric tunability n that is defined as the ratio of the relative permittivity in the absence of an electric field to that at the maximum electric field strength, which is possible only in the paraelectric state near Curie temperature T_c. At room temperature, these conditions are realized for compounds with $0.45 < x < 0.65$.

Another major degree of freedom is the mechanical state of the BSTO film. It influences film's electromagnetic properties both directly and indirectly through shifting the Curie temperature T_c of the ferroelectric–paraelectric phase transition. This emphasizes the importance of the choice of the substrate inducing mechanical stress in the BSTO layer.

That is why we have grown BSTO films on various substrates including YIG/GGG (the basic one, unavoidable for implementation of the *bi-layer extrinsic BSTO/YIG configuration*), sapphire (α-Al_2O_3), lanthanum aluminate $LaAlO_3$ (LAO), and alumina, with thicknesses in the range 300–500 μm. BSTO films with x in the range from 0.45 to 0.65 were deposited by RF magnetron sputtering and had thicknesses $h = 0.5$–1.5 μm.

That is why, at the first stage we had to choose the optimal substrate for ameliorating performance of the investigated structures, especially in terms of the above-mentioned electric tunability n. The results of the preliminary analysis (see Table 1), discussed in more detail in the following two sections, have shown that the sapphire (α-Al_2O_3) substrate, corresponding to a higher Curie temperature, is better suited for microwave applications and thus it was chosen for fabrication of the Mn-doped BSTO single layers representing the principal *intrinsic configuration* under study. For these experiments, we have chosen the BSTO films with $x = 0.5$. This well-balanced symmetric stoichiometry has proved optimal for microwave applications. The content of manganese (doping rate) in the BSTO films was varied for two sets of samples within the range from 0 to 2 mol% for the first one and from 10 to 20 mol% for the second one. It should be noted that the sputtering technique employed in the fabrication of Mn-doped BSTO single layers makes it much easier to incorporate these films into hybrid integrated structures, than in the case of single-crystal dielectric ferrites prepared by liquid-phase epitaxy. In other words, technologically, the intrinsic configuration, not requiring costly liquid-phase epitaxy, is far more attractive.

For experimental investigation of dielectric properties, planar capacitors were formed on the structures of both configurations (see Fig. 1) by thermal evaporation followed by wet photolithography. They are made of copper with a chromium sublayer (Cu–Cr). The gap width d in the planar capacitors was in the range of 3–7 μm and the gap length l varied from 250 to 850 μm.

Structural characterization

Structural characterization of the samples under study was based on X-ray diffraction analysis (XRD) [14]. As the first step, we have undertaken a study of the influence of the substrate on the major structural and dielectric properties of the BSTO film in order to optimize sample preparation procedure for both configurations, namely the Mn-doped BSTO

Table 1 Lattice parameter, Ba/Sr ratio, film thickness, temperature of ε maximum, dielectric permittivity, dielectric losses, tunability

Substrate	LAO	α-Al_2O_3	Alumina	YIG
a (Å)	3.982	3.954	3.966	3.962
x	0.55	0.55	0.6	0.6
h (μm)	0.950	0.75	0.4	0.4
T_m (K)	220	280	260	265
ε [300 K, 0 V]	2200	1545	820	1910
tanδ [300 K, 0 V]	0.005	0.011	0.009	0.017
n [295 K, 30 V/μm]	1.4	2.1	1.74	1.43

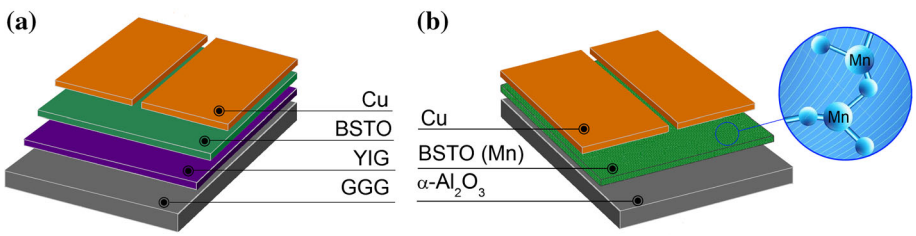

Figure 1 Planar capacitors based on artificial multiferroic structures: **a** extrinsic BSTO/YIG bi-layer and **b** intrinsic Mn-doped BSTO single layer.

monolayer on a sapphire substrate (α-Al_2O_3) and BSTO/YIG bi-layer. In order to describe the influence of the YIG film on the properties of the bi-layers, the following substrates were chosen LAO, α-Al_2O_3, alumina, and YIG.

The data from X-ray diffraction analysis, namely values of the lattice constants *a*, are summarized in the upper part of Table 1. It is known that α-Al_2O_3 has a hexagonal crystal structure, alumina substrates are polycrystalline, LAO substrates have the perovskite structure, and YIG is cubic. The BSTO films on all substrates are polycrystalline with preferred orientation (100). The Ba/Sr ratios in the table correspond to the compositions having the best possible combination of major dielectric characteristics, namely low dielectric loss tangent tanδ, high values of the relative permittivity ε, and electric tunability *n* for operation at room temperature that are given for reference in the lower part of Table 1.

Some interesting specific features of the process of film formation at the film–substrate interface have also been revealed by analysis of X-ray Photoelectron Spectroscopy (XPS) spectra of a BSTO/YIG/GGG bi-layer structure (see Fig. 2), which is of particular importance in the context of this research.

Thus, it was shown that within the 0.4-μm BSTO film there exists a 0.035-μm-thin inhomogeneous layer at the BSTO/YIG interface characterized by oxygen deficiency and the nonstoichiometric ratio between the cation components of the BSTO. This border layer is of intermediate nature and hardly has ferroelectric properties. The distribution of all the main components in the rest of the BSTO film can be regarded as homogeneous. As for the interdiffusion, residual traces of Y were found in BSTO. On the other hand, Ba, Sr, and Ti are observed to penetrate into the YIG film but only to a depth not exceeding 0.1 μm. An interfacial layer of this thickness in a 8-μm YIG film has practically no effect on its magnetic properties. This was confirmed by measurements of the magnetic dissipation parameter ΔH (half-width of the ferromagnetic resonance line) which did not change after deposition of the BSTO on a YIG film.

As the second step, XRD analysis was used to study the $Ba_{0.5}Sr_{0.5}TiO_3$/α-Al_2O_3 structures with relatively low Mn doping rate in the range of 0–2 mol%. The results obtained from XRD allow for concluding that with the Mn concentration increasing up to 2 mol%, the lattice parameter grows from 3.947 up to 3.951 Å. The results obtained at these two steps for

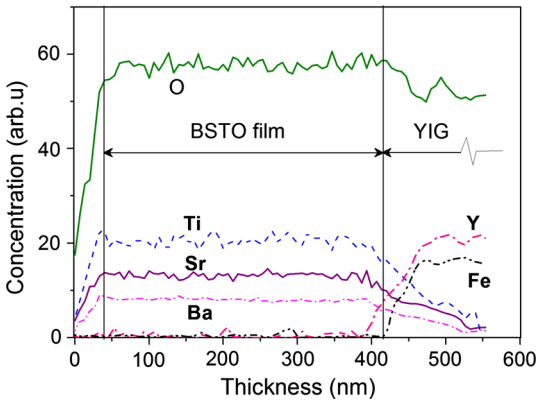

Figure 2 XPS spectrum of the BSTO/YIG bi-layer.

BSTO on various substrates and BSTO/α-Al_2O_3 with low Mn doping rate are typical and will be used like reference for further investigation and analysis of the influence of higher Mn doping rates on structural properties.

Finally, XRD analysis was used for investigation of $Ba_{0.5}Sr_{0.5}TiO_3$/α-Al_2O_3 structures with relatively high Mn concentration from 10 to 20 mol%. All the samples belonging to this series have been XRD characterized. A typical XRD spectrum for the BSTO film with 15 mol% Mn doping, which as it will be shown below to have the highest magnetic tunability, is shown in Fig. 3. As can be seen, the investigated structure contains several contributions with different Ba/Sr ratios. The main one is Ba/Sr = 0.5/0.5 with a lattice constant $a = 3.947$ Å. Furthermore, additional manganese-containing phases $Ba(Ti_{0.5}Mn_{0.5})O_3$ with $a = 5.689$ Å and MnO_2 with $a = 4.327$ Å were observed in the X-ray diffraction pattern in Fig. 3. The concentration of these phases increases

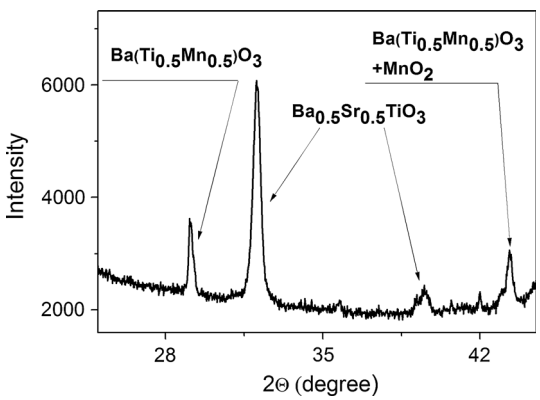

Figure 3 X-ray diffraction pattern of a BSTO film with 15 mol% of Mn.

proportionally with variation of the Mn doping rate. The X-ray diffraction patterns of samples with 20 mol% Mn demonstrated an increase in the number of phases, with Ba/Sr ratios different from the initial and a substantial rise in the content of MnO_2.

Dielectric properties and dual tunability: experimental results

It is common knowledge that BSTO solid solutions do not exhibit any dispersion of the relative permittivity ε in a vast frequency range from 10^2 to 10^{11} Hz [15, 16]. Thus, capacitance–voltage (C–V) characteristics, dielectric loss tangent tanδ, and their temperature dependences were taken at a frequency of 1 MHz. An automated digital bridge (with a relative capacitance measurement error of 0.01 %) was used to measure the impedance of the planar capacitors created on experimental structures. The amplitude of the probing signal of the bridge was about 0.5 V, and the bias voltage was varied within $V = \pm 200$ V. The relative permittivity was calculated from the capacitance of the planar structure measured for temperatures in the interval from 77 to 300 K [13, 17]. DC conduction currents were registered with an electrometer in the range from 10^{-13} to 10^{-5} A. The confidence interval in these measurements did not exceed 5 %.

Temperature dependences $C(T)$ of the capacitance of the planar structures based on the BSTO films on various substrates are given in Fig. 4. All the curves demonstrate a characteristic maximum at a temperature T_m in the vicinity of the phase transition. The parameter T_m in BSTO films is affected by several factors that fall into two major categories [18] related either to the stoichiometry composition, such as Ba/Sr cation component ratio (value of x) and oxygen content (concentration of oxygen vacancies), or to their mechanical state, namely the lattice mismatch between the substrate and film materials and difference in the thermal expansion coefficients of these materials.

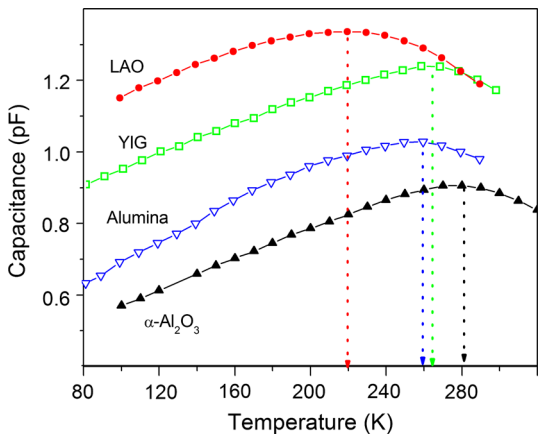

Figure 4 Temperature dependences of the capacitance of layered structures grown on various substrates: LAO, α-Al_2O_3, alumna, and YIG.

Both the lattice mismatch between the substrate and film and the difference in their thermal expansion coefficients give rise to deformation in BSTO films, estimated in this study by the relative change η in the lattice parameter in a given film material (a) with respect to its unstressed single-crystal value (a_{ref}):

$$\eta = (a - a_{ref})/a_{ref}. \quad (1)$$

It is known that the lattice constant a_{ref} grows linearly with increasing x in BSTO solid solutions. In particular, an increase in x from 0.5 to 0.65 induces a growth in the lattice constant a_{ref} from 3.947 to 3.990 Å. Thus, it follows from comparison of the lattice constants obtained by XRD in Table 1 and the corresponding reference unstressed single-crystal values that, for example, the strain in BSTO films grown on LAO substrates, varies accordingly $\eta = (4.2–6.2)\ 10^{-3}$, being of tensile nature. At the same time, for the BSTO films grown on α-Al_2O_3 substrates, a compressive strain estimated at $\eta = -(4.2–3.1)\ 10^{-3}$ is observed. Most of BSTO films grown on alumina substrates exhibit almost a negligible deformation compared to the case of the α-Al_2O_3 substrate. Similar behavior, a weak compressive strain, was observed in the case of YIG/GGG substrates. Importantly, the shift in T_m on the temperature dependence of the capacitance for each particular sample scales with the mechanical strain (see Fig. 4) within it.

For example, the temperature dependence for the sample on the alumina substrate, in which the strain is nearly zero has the maximum at $T_m = 260$ K. For the BSTO/LAO samples in which tensile deformations were observed, T_m is shifted to *lower* temperatures. Correspondingly, for the BSTO/α-Al_2O_3 samples with compressive deformations, this temperature is pushed by 20–40 K to *higher* temperatures. Not surprisingly, the $C(T)$ dependence for the BSTO/YIG/GGG multilayer structure has a maximum at

$T_m = 265$ K, which is close to a nearly unstrained BSTO/alumina structure.

Preliminary characterization accomplished, we proceed to the principle part of this paper, namely study of the magnetodielectric effect, i.e., the influence of the magnetic field on the dielectric permittivity in intrinsic multiferroic monolayers synthesized via doping of a BSTO paraelectric matrix with paramagnetic ions of manganese in concentrations sufficient for appearance of magnetic properties.

As it was shown earlier in Ref. [19–21], addition of MnO_2 to BSTO films at a rate of 1–2 mol% leads to a significant change in their dielectric characteristics. Although the principal physical mechanism behind these changes, compensation of positively charged oxygen vacancies, has already been identified, there are still questions to be answered. Thus, it has turned out that this effect is very technology dependent and differs considerably in bulk single-crystal samples, ceramic layers, and thin films (grown by different deposition techniques and on different substrates).

That is why two batches of Mn-doped BSTO films were prepared, namely a low doping rate series with manganese concentration in the range of 0–2 mol% (the reference series) and a high concentration in the range of 10–20 mol%. We have chosen the sapphire substrate as the best suited for microwave applications (excellent tunability, high permittivity, and satisfactory tanδ).

As shown in the previous section, with the Mn content increasing up to 2 mol%, the lattice parameter grows up, which pushes the characteristic temperature T_m down by 30–40 K with respect to pure samples (see Table 2; Fig. 5). This means that the film shifts away from the phase transition, thus becoming "more paraelectric." The latter statement can be formulated otherwise. Any dielectric material in the ferroelectric phase is characterized by high values of dielectric permittivity and microwave losses with respect to its paraelectric phase. That is why paraelectric properties at room temperature are more pronounced (relatively low values of the dielectric permittivity and microwave losses) in a material with a low temperature of para-ferroelectric phase transition T_m. In this case, the investigated dielectric is "far" from its ferroelectric "incarnation." That is why the dielectric loss tangent becomes substantially smaller (tan$\delta \leq 0.002$), and the relative permittivity ε and electric tunability n decrease (see Table 2).

Table 2 Film thickness, temperature of ε maximum, tunability, dielectric permittivity, dielectric losses

Mn content (mol%)	0	1	2
h (μm)	0.5	0.65	0.65
T_m (K)	260	250	230
n [295 K, 30 V/μm]	1.74	1.67	1.3
ε [295 K, 0 V]	1500	2000	900
tanδ [295 K, 0 V]	0.01	0.012	0.001–0.002

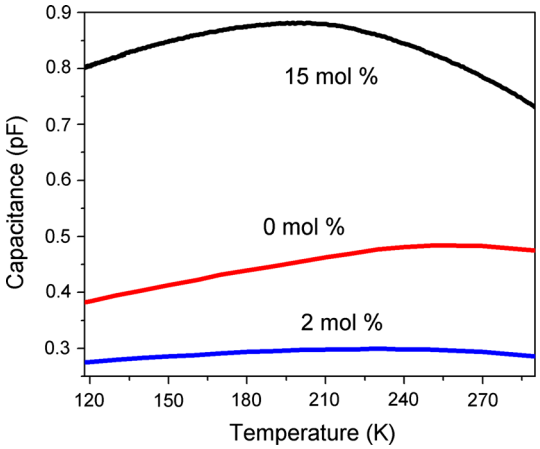

Figure 5 Temperature dependences of the capacitance of the BSTO/α-Al_2O_3 samples with various Mn concentrations: 0, 2, and 15 mol%.

Note that another feature observed is the inversion of the tan$\delta(V)$ dependence: an electrical bias leads to a slight increase in tanδ from 0.001 to 0.002, rather than to a sharp decrease from 0.01 to 0.002 as in pure BSTO films [21]. The fact that tanδ grows with increasing voltage V indicates that there is no loss mechanism due to charged defects in these samples [22]. No effect of a magnetic field $H = 2000$ Oe on the dielectric characteristics of structures with the Mn doping rate in the range of 0–2 mol% was found.

To conclude, our investigation of the reference low concentration series, on the one hand, confirms some previously reported general tendencies and, on the other hand, provides us with important numerical parameters essential for understanding of the results obtained on samples with high Mn concentration. These are summarized in Table 3. More specifically, it shows the results of a study of BSTO/α-Al_2O_3 structures with the Mn content increasing from 10 to 20 mol%. As shown in the previous section, the lattice constants of the manganese-containing compositions substantially exceed the parameters of the

Table 3 Film thickness, temperature of ε maximum, tunability, dielectric permittivity, dielectric losses, resistance

Mn content (mol%)	10	15	20
h (μm)	0.82	0.98	1.0
T_m (K)	166	190	200
n [295 K, 30 V/μm]	1.33	2.05	1.33
ε [295 K, 0 V]	340	650	413
tanδ [295 K, 0 V]	0.003	0.001	0.002
R (Ohm)	2×10^{10}	10^{11}	2×10^{9}

BSTO lattice, which makes it possible to convert the already existing due to the BSTO/substrate lattice parameter mismatch compressive deformation into a pronounced tensile deformation. As a result, the maximum T_m in the temperature dependence of the capacitance of the BSTO:Mn samples is shifted to lower temperatures by more than 50 K in comparison with purely BSTO samples (see Table 3; Fig. 5). Note that the difference in the capacitance values in Fig. 5 is due to the planar capacitor form factor.

The study of the dielectric characteristics of the BSTO:Mn sample shows that high concentration of Mn comes at a price: dielectric permittivity drops dramatically, typically 4–5 times (Table 3). At the same time, microwave losses, described by tanδ, are noticeably improved. This is not surprising, since with lower temperatures of the phase transition in highly compressed films, the actual state of the film at room temperature "shifts away" from the ferroelectric phase, characterized by extra-high values of epsilon, including both its real and imaginary parts.

Neither major dielectric parameter has shown monotonous growth/decrease as a function of the Mn concentration and it is the 15 mol% sample that has demonstrated by far the best dielectric behavior, i.e., the largest relative permittivity $\varepsilon = 650$–670, unmatched electric tunability $n = 1.9$–2.0, and the lowest losses tan$\delta = 0.001$.

The last part of this experimental study was dedicated to the investigation of the *magnetic tunability* of the BSTO samples with high Mn doping rate. By *magnetic tunability* we mean the influence of the magnetic field on the dielectric properties of the structure under investigation described by the following formula:

$$m = (\varepsilon(H) - \varepsilon(0))/\varepsilon(0) \times 100\,\%. \quad (2)$$

Typical C–V characteristics, obtained on the 15 mol% Mn sample grown on a α-Al_2O_3 substrate, in the absence of external magnetic field (solid line) and with a magnetic field $H = 2000$ Oe applied (dash line) are presented in Fig. 6. This figure shows the influence of a magnetic field $H = 2000$ Oe. It should be stressed that the 15 % Mn concentration has proved optimal not only for dielectric behavior but also in terms of *magnetic tunability* $m = 3$ %. Thus, no effect of the magnetic field on the C–V characteristics of the structures was observed for lower concentrations and, surprisingly, with Mn content of 20 mol%, the effect of the magnetic field on C–V characteristics decreased, although still being noticeable.

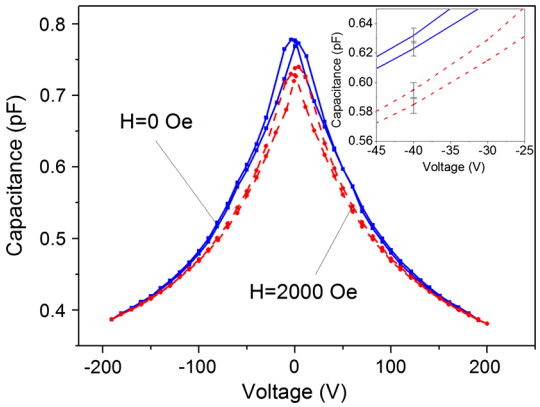

Figure 6 C–V characteristics of the capacitor based on BSTO/α-Al_2O_3 with 15 mol% of Mn dopant in the absence of external magnetic field (*solid line*) and with a magnetic field $H = 2000$ Oe (*dash line*).

The 15 mol% Mn concentration proved to be special also in terms of conductivity of the Mn-doped samples. The latter decreases with the Mn content reaching its lowest value for 15 mol%, and then starts to rise steeply (see Fig. 7).

Table 3 lists the sample resistances estimated from the ohmic portions of the current–voltage characteristics. The sharp increase in conductivity for samples containing 20 mol% Mn impurity is due to the appearance of conducting Mn and MnO_2 phases, confirmed by X-ray data. Comparison of the C–V characteristics and current–voltage characteristics of samples with different contents of magnetic ions has confirmed that the optimum content of Mn in $Ba_{0.5}Sr_{0.5}TiO_3$ films is 15 mol%. The increase of Mn concentration up to 15 mol% induces a decrease of the conductivity, whereas in contrast magnetic tunability is increased, which confirms stronger magnetoelectric coupling.

The second type of multiferroic materials investigated in this paper is a BSTO/YIG bi-layer on a GGG

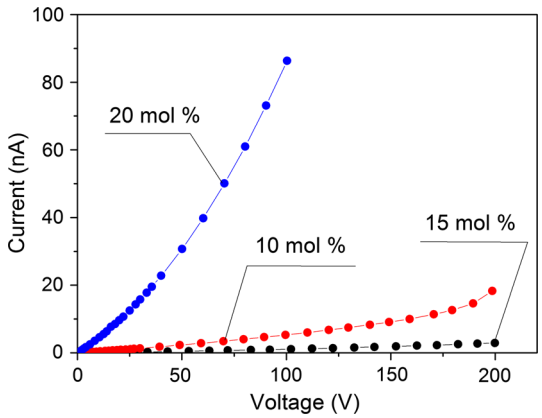

Figure 7 Current–voltage characteristics of the BSTO/α-Al_2O_3 samples with various Mn concentrations: 10, 15, and 20 mol%.

substrate. Correspondingly, C–V characteristics were measured (see Fig. 8) both in the absence of external magnetic field (solid line in Fig. 8) and with a magnetic field $H = 2000$ Oe applied (dash line in Fig. 8). Application of a magnetic field shifts the characteristic maximum on the temperature dependence $C(T)$ to lower temperatures which corresponds to the appearance of tensile deformations. Note that prior to application of an external magnetic field to the BSTO/YIG/GGG structure, no mechanical stress has been detected in it (see Fig. 4). The maximal value of *magnetic tunability* m is equal to 6 %, and decreases with an increase of electric voltage down to 0.5 % at $V = 200$ V.

To finalize this particular analysis, it would be worthwhile to outline the major physical mechanisms that are involved in the magnetodielectric coupling in both configurations, intrinsic and extrinsic. Let us begin with the Mn-doped BSTO single layers characterized by natural magnetodielectricity.

The magnetoelectric effects in multiferroic structures are traditionally described [3] in Landau theory by writing the free energy F of the system in terms of the applied magnetic H and electric E fields. While the more discussed magnetoelectric coupling is described by the bilinear in H and E terms, higher order terms in this expansion correspond to magnetodielectric effect [23, 24]. The biquadratic seems to be the most relevant candidate since it produces a scalar contribution to the free energy for all systems, regardless of the symmetry of the underlying lattice or magnetic structure. Since E is a polar vector and M is an axial vector terms, linear in M will typically not yield a scalar and so vanish from the free energy expansion [23]. Theoretically, this is possible for some low-symmetry crystals. However, all our measurements of the magnetodielectric properties for investigated structures were made at room temperature in which case the samples are in the paraelectric phase characterized by the highest symmetry possible in the crystal under investigation, namely cubic.

Now let us proceed to the second YIG/BSTO bilayer configuration, demonstrating artificial extrinsic magnetodielectric coupling. In such structures, it is a two-step process as always is the case with extrinsic ferroics. Thus at the first stage, the external magnetic field induces a static stress in the ferromagnetic YIG film via magnetostriction. This deformation is transferred to the paraelectric BSTO layer, in which it induces a change of the dielectric permittivity. In the particular context of this paper, the modulation of permittivity by stress should be regarded in the following way. As shown earlier in this paper, mechanical stress shifts the Curie temperature, which in turn results in a corresponding shift in the value of the permittivity. More specifically, compressive deformations increase the Curie temperature and thus lead to higher values of the dielectric permittivity. Conversely, tensile deformations decrease the latter.

To conclude this experimental section, we would like especially to emphasize the importance of the results obtained in its second part where we have revealed the most significant feature common to both configurations, namely the dual tunability. This novel functionality consists in a possibility of "tuning" the dielectric characteristics both by means of the electric and magnetic fields.

Discussion

The pivotal parameter in this discussion is the characteristic temperature T_m, corresponding to maxima in temperature dependences, which is very close to the Curie point T_C. The latter separates the ferroelectric and paraelectric states and is effectively controlled by the stoichiometry of the BSTO solid solutions. Since we are interested in microwave applications, the Ba/Sr ratio has been chosen accordingly $x = 0.5$. At the same time, closeness to the ferromagnetic state intensifies sensitivity of the paramagnetic material to external fields which means better tunability. Moreover, absolute values of the

dielectric permittivity also increase. Unfortunately, this concerns its imaginary part as well, which means a nonnegligible deterioration of tanδ, describing microwave losses.

It is known that mechanical stresses may noticeably affect the temperature dependence of the relative permittivity $\varepsilon(T)$. The latter scales with the experimentally observed $C(T)$ functions and thus can be extracted directly from the experimental data. Typically, this mechanism leads to a temperature shift on the order of several tens of degrees in either direction. Given the proximity of the Curie point, this relatively modest shift can lead to considerable changes to microwave dielectric properties of BSTO solid solutions. In other words, mechanical stress can be considered as an additional effective instrument for "fine tuning" of BSTO-based functional materials with a given stoichiometry parameter x.

Our theoretical analysis is based on the Ginsburg–Devonshire expansion of the free energy in powers of polarization and mechanical stress at low electric field strengths. We can restrict our consideration to the first two terms and, having differentiated with respect to the degree of polarization, obtain the following dependence of the inverse relative permittivity on temperature and mechanical stresses [25]:

$$(\varepsilon_0 \cdot \varepsilon)^{-1} = (\varepsilon_0 \cdot C_C)^{-1}(T - T_C + \varepsilon_0 \cdot C_C \cdot G \cdot U). \quad (3)$$

Here C_C is the Curie–Weiss constant, and G and U are components of the electrostriction and mechanical stress tensors, respectively. The last two terms in this expression can be regarded as an effective value of the Curie temperature $T^* = T_C - \varepsilon_0 C_C G U$. Then, the effective Curie temperature $T^* < T_C$ in the case of tensile deformations ($U > 0$) and $T^* > T_C$ for compressive deformations ($U < 0$). The experimentally observed evolution of the maximum temperature T_m in the $C(T)$ dependences for samples with different mechanical stress signs is correlated with the behavior of T^*. Thus, we can conclude that there always are tensile deformations in the BSTO films on LAO substrates, and compressive deformations are the most probable in the BSTO films on α-Al_2O_3 substrates. The lowest stresses occur in the BSTO films grown on alumina substrates and YIG films (see Fig. 2; Table 1). Unstrained films or films with weak tensile deformations are more preferable as regards the values of ε and tanδ (see Table 1).

It is well known that dopants such Mn typically occupy the B site of the ABO_3 perovskite structure [26] that was also confirmed in our work. It is also known that titanium mostly has a valence (+4) in solid solutions but may also exhibit a valence (+3) [27]. In barium titanate films, a modified phase $Ba(Ti^{+3}_{0.48}Ti^{+4}_{0.52})O_3$ with an imperfect tetragonal structure is formed. Manganese is also a variable-valence element: Mn^{+4}, Mn^{+3}, Mn^{+2}. At the same time, with decreasing valence of manganese ions, their ionic radius grows from 0.052 to 0.083 nm. For titanium ions, the tendency for variation of the ionic radius with decreasing valence is the same: Ti^{+4} has an ionic radius of 0.062 nm and that of Ti^{+3} is 0.066 nm [21]. If Mn^{+2} occupies the position of Ti^{+4}, this gives rise to a tensile deformation in the crystal lattice and to an additional shift of the maximum (T_m) in the temperature dependence of the capacitance to lower temperatures, with respect to undoped films (see Fig. 5). In addition, the charge model of compounds of this kind can be represented as $(Ba_xSr_{1-x})^{+2}Ti^{+4}_{1-y}[Mn_{Ti}]^{-2}_y O^{-2}_{3-z}[V_o]^{+2}_z$ ([V_o] are oxygen vacancies). In this case, the oxygen vacancies, which are always present in BSTO compounds, give rise to charged defects responsible for the large values of tanδ (samples with 0 and 1 mol% in Table 2) [21, 28]. Due to compensation of oxygen vacancies [V_o] by $[Mn_{Ti}]^{-2}$, values of the dielectric loss tangent decrease (samples with 2 mol% in Table 2 and 10–20 mol% in Table 3).

It should also be noted that, leaving the BSTO lattice, Sr^{+2} whose ionic radius is 0.118 nm (which always somewhat exceeds the ionic radius of Mn in

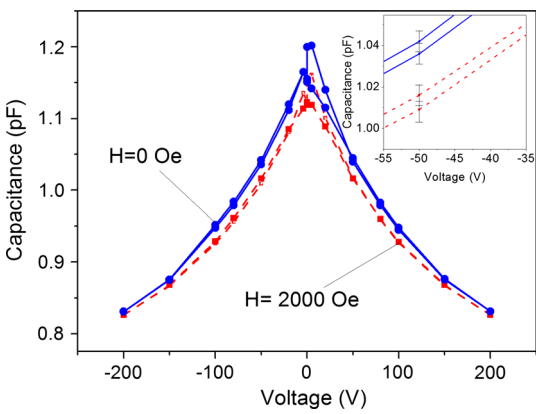

Figure 8 C–V characteristics of the capacitor based on BSTO/YIG bi-layers measured in the absence of external magnetic field (*solid line*) and with a magnetic field $H = 2000$ Oe (*dash line*).

any valence state), might give rise to compressive deformations. However, this is not the case. The additional manganese-containing phase $Ba((Ti_{0.5}Mn_{0.5})O_3)$ and the MnO_2 phase, both detected by X-ray analysis, have lattice constants $a = 5.689$ Å and $a = 4.327$ Å, respectively. This also shifts the temperature maxima T_m to lower temperatures, compared with undoped samples. At the same time, these weak compressive deformations at the BSTO/α-Al_2O_3 interface are excessively compensated for by tensile deformations of varied nature.

Structural analysis of heavily Mn-doped BSTO has revealed an increasingly multiphase character of the structure. This allows explaining certain features experimentally observed. Thus, it was demonstrated in the study of the C–V characteristics of multiferroic structures that raising the Mn content to 20 mol% leads to a sharp rise in the conductivity of the samples due to the large amount of conducting MnO_2 and Mn phases. This, in turn, reduces the relative permittivity and makes tanδ larger. The optimal content of the Mn additive, as regards the dielectric properties (values of ε, tanδ, tunability n, and resistance R in Table 3), is 15 mol%.

Both methods for obtaining materials with multiferroic properties enable an additional control over the relative permittivity and tunability by the magnetic field. The effect of the magnetic field on these structures is not strong (see Figs. 6, 8), because BSTO and YIG films exhibit a weak electrostrictive effect. If other films, e.g., PZT, are used as a ferroelectric and a ferromagnetic, then the effect of the magnetic field on the dielectric properties of the structures can be considerably enhanced. At the same time, application of the structures we studied at microwaves does not require multifold changes in dielectric properties under the influence of the magnetic field. The latter can be used to fine-tune by 3–5 % the microwave elements. The characteristics shown in Fig. 6 demonstrate that the multiferroic structures can be 100 % controlled by an electric field and 3 % tuned by a magnetic field.

Conclusions

Thus, in this paper we have experimentally confirmed the feasibility of BSTO-based functional multiferroic materials, both intrinsic, in the form of Mn-doped BST films, and extrinsic, in the form of BST/YIG bi-layers. More specifically, in the latter case a new functionality of BST/YIG structures has been revealed. In addition to previously investigated electrodynamic coupling between spin-waves in the YIG film and slow modes in the BST layer, another type of interaction referred to as magnetodielectric effect, i.e., influence of the magnetic field on the dielectric permittivity, has been discovered. While the electrodynamic coupling is efficient only if phase synchronism between the interacting modes is observed, the magnetodielectric interaction is of more general nature. Given the fact that BST is naturally electrically nonlinear, the structures considered can boast dual tunability. The latter applies also to the intrinsically double-ferroic Mn-doped BSTO single layers. It is experimentally shown that while low Mn doping rate (1–2 mol%) in BSTO improve dielectric properties, increase of the doping rate up to 15 mol% enables an additional 3 % tuning of the dielectric permittivity by an external magnetic field. Both structures are promising for microwave devices, the attractiveness of each one depending on the specificity of the particular application.

Acknowledgements

The samples were prepared at the St. Petersburg Electrotechnical University with support of the Russian Science Foundation (Grant 14-12-01296). The measurements and investigations were supported in part by grant of the President of the Russian Federation for young scientists and PhDs MK-6229.2015.8, the Government of the Russian Federation (Grant 074-U01), and the Russian Foundation of Basic Research (Project No. 16-32-00715 mol_a).

References

[1] Cheong SW, Mostovoy M (2007) Multiferroics: a magnetic twist for ferroelectricity. Nat Mater 6:13–20. doi:10.1038/nmat1804

[2] Spaldin NA, Cheong SW, Ramesh R (2010) Multiferroics: past, present, and future. Phys Today 63:38–43. doi:10.1063/1.3502547

[3] Eerenstein W, Mathur ND, Scott JF (2006) Multiferroic and magnetoelectric materials. Nature 442759:759–765. doi:10.1038/nature05023

[4] Fernandes Vaz CA, Staub U (2013) Artificial multiferroic heterostructures. J Mater Chem C 1:6731. doi:10.1039/C3TC31428F

[5] Nan CW, Bichurin MI, Dong S, Viehland D, Srinivasan G (2008) Multiferroic magnetoelectric composites: historical perspective, status, and future directions. J Appl Phys 103:031101. doi:10.1063/1.2836410

[6] Özgür Ü, Alivov Y, Morkoç H (2009) Microwave ferrites, part 2: passive components and electrical tuning. J Mater Sci 20:911–952. doi:10.1007/s10854-009-9924-1

[7] Sun NX, Srinivasan G (2012) Voltage control of magnetism in multiferroic heterostructures and devices. Spin 2:1240004. doi:10.1142/S2010324712400048

[8] Vopson MM (2015) Fundamentals of multiferroic materials and their possible applications. Crit Rev Solid State Mater Sci 40:223–250. doi:10.1080/10408436.2014.992584

[9] Subramanyam G, Cole MW, Sun NX, Kalkur TS, Sbrockey NM, Tompa GS, Guo X, Chen C, Alpay SP, Rossetti GA Jr, Dayal K, Chen L-Q, Schlom DG (2013) Challenges and opportunities for multi-functional oxide thin films for voltage tunable radio frequency/microwave components. J Appl Phys 114:191301. doi:10.1063/1.4827019

[10] Gurevich AG, Melkov GA (1996) Magnetization oscillations and waves. CRC Press, Boca Raton

[11] Stancil DD, Prabhakar A (2009) Spin waves. Springer, Luxembourg

[12] Tagantsev AK, Sherman VO, Astafiev KF, Venkatesh J, Setter N (2003) Ferroelectric materials for microwave tunable applications. J Electroceram 11:5–66. doi:10.1023/B:JECR.0000015661.81386.e6

[13] Vendik OG, Hollmann EK, Kozyrev AB, Prudan AM (1999) Ferroelectric tuning of planar and bulk microwave devices. J Supercond 12:325–338. doi:10.1023/A:1007797131173

[14] Noyan IC, Huang TC, York BR (1995) Residual stress/strain analysis in thin films by X-ray diffraction. Crit Rev Solid State Mater Sci 20:125–177. doi:10.1080/10408439508243733

[15] Houzet G, Burgnies L, Velu G, Carru JC, Lippens D (2008) Dispersion and loss of ferroelectric $Ba_{0.5}Sr_{0.5}TiO_3$ thin films up to 110 GHz. Appl Phys Lett 93:3–5. doi:10.1063/1.2969469

[16] Nenasheva EA, Kanareikin AD, Dedyk AI, Pavlova YV (2009) Electrically controlled BST-Mg ceramic components for applications in accelerator technology. Phys Solid State 51:1557–1560. doi:10.1134/S1063783409080046

[17] Vendik OG, Zubko SP, Nikol'skii MA (1999) Modeling and calculation of the capacitance of a planar capacitor containing a ferroelectric thin film. Tech Phys 44:349–355. doi:10.1134/1.1259300

[18] Karmanenko SF, Dedyk AI, Isakov NN, Sakharov VI, Semenov AA (1999) Component composition and strain of barium–strontium titanate ferroelectric films. Tech Phys Lett 25(10):780–783. doi:10.1134/1.1262633

[19] Yuan Z, Lin Y, Weaver J, Chen X, Chen CL, Subramanyam G et al (2005) Large dielectric tunability and microwave properties of Mn-doped (Ba, Sr)TiO_3 thin films. Appl Phys Lett 87:1–3. doi:10.1063/1.2089181

[20] Wu H, Barnes FS (1998) Doped $Ba_{0.6}Sr_{0.4}TiO_3$ thin films for microwave device applications at room temperature. Integr Ferroelectr 22:291–305. doi:10.1080/10584589808208050

[21] Karmanenko SF, Dedyk AI, Isakov NN, Gordeichuk AS, Semenov AA, Ter-Martirosyan LT et al (2001) Study of the effect of manganese impurities on dielectric characteristics of BSTO films. Tech Phys 46:498–502. doi:10.1134/1.1365480

[22] Vendik OG, Ter-Martirosyan LT (1999) Electrostrictive mechanism of microwave losses in a planar strontium titanate film capacitor. Tech Phys 44:954–959. doi:10.1134/1.1259412

[23] Lawes G, Kimura T, Varma CM, Subramanian MA, Rogado N, Cava RJ, Ramirez AP (2009) Magnetodielectric effects at magnetic ordering transitions. Prog Solid State Chem 37:40–54. doi:10.1016/j.progsolidstchem.2009.08.001

[24] Manfred F (2005) Revival of the magnetoelectric effect. J Phys D 38:123. doi:10.1088/0022-3727/38/8/R01

[25] Prudan AM, Gol'man EK, Kozyrev AB, Loginov VE (1997) Properties of strontium titanate in the $SrTiO_3/CeO_2/Al_2O_3$ multilayered structure. Phys Solid State 39(6):920–924. doi:10.1134/1.1130156

[26] Cole MW, Ngo E, Hubbard C, Hirsch SG, Ivill M, Sarney WL, Zhang J, Alpay SP (2013) Enhanced dielectric properties from barium strontium titanate films with strontium titanate buffer layers. J Appl Phys 114:164107. doi:10.1063/1.4827421

[27] Yoon SH, Randall CA, Hur KH (2010) Difference between resistance degradation of fixed valence acceptor (Mg) and variable valence acceptor (Mn)-doped $BaTiO_3$ ceramics. J Appl Phys 108:1–9. doi:10.1063/1.3480992

[28] De Araujo CP (1996) Ferroelectric thin films: synthesis and basic properties. Taylor & Francis, Abingdon